NIH Public Access
Author Manuscript
Dent Mater. Author manuscript; available in PMC 2013 February 1.

Published in final edited form as:
Dent Mater. 2012 February ; 28(2): 113–122. doi:10.1016/j.dental.2011.09.010.

Effects of SiO_2 and ZnO doping on mechanical and biological properties of 3D printed TCP scaffolds

Gary A. Fielding, **Amit Bandyopadhyay**, and **Susmita Bose**[1]
W. M. Keck Biomedical Materials Research Laboratory School of Mechanical and Materials Engineering Washington State University Pullman, WA 99164-2920, USA

Abstract

Objectives—To evaluate the effects of SiO_2 (0.5 wt %) and ZnO (0.25 wt %) dopants on the mechanical and biological properties of tricalcium phosphate (TCP) scaffolds with three dimensionally (3D) interconnected pores.

Methods—Scaffolds were created with a commercial 3D printer. Post sintering phase analysis was determined by x-ray diffraction. Surface morphology of the scaffolds was examined by field emission electron microscopy. Mechanical strength was evaluated with a screw driven universal testing machine. MTT assay was used for cellular proliferation characteristics and cellular morphology was examined by field emission electron microscopy.

Results—Addition of dopants into TCP increased the average density of pure TCP from 90.8 ± 0.8% to 94.1 ± 1.6% and retarded the β to α phase transformation at high sintering temperatures, which resulted in up to 2.5 fold increase in compressive strength. *In vitro* cell-materials interaction studies, carried out using hFOB cells, confirmed that the addition of SiO_2 and ZnO to the scaffolds facilitates faster cell proliferation when compared to pure TCP scaffolds.

Significance—Addition of SiO_2 and ZnO dopants to the TCP scaffolds showed increased mechanical strength as well as increased cellular proliferation.

Keywords

β-tricalcium phosphate; porous scaffold; three dimensional printing; doped calcium phosphates; bone tissue engineering

1. Introduction

Currently in dental applications, synthetic materials such as amalgam, resin, gutta-purcha, dentures and metal implants have been used to treat conditions such as caries, pulpits, periodontal disease and trauma. These repair methods are incapable of reproducing the natural function of the lost tissue and lead to mechanical deficiencies and reduced tooth vitality [1-2]. Long term studies have shown that these treatments may have an effect on a patient's masticatory and digestive functions [3-4]. In the past 15 years, due in part to the shortcomings of these materials, there has been a growing interest in the investigation of synthetic bone alternatives as well as manufacturing methods. Advances in rapid

© 2004 Academy of Dental Materials. Published by Elsevier Ltd. All rights reserved.

[1] Corresponding Author Fax: (509) 335-4662 sbose@wsu.edu.

Publisher's Disclaimer: This is a PDF file of an unedited manuscript that has been accepted for publication. As a service to our customers we are providing this early version of the manuscript. The manuscript will undergo copyediting, typesetting, and review of the resulting proof before it is published in its final citable form. Please note that during the production process errors may be discovered which could affect the content, and all legal disclaimers that apply to the journal pertain.

NIH-PA Author Manuscript
NIH-PA Author Manuscript
NIH-PA Author Manuscript

NIH-PA Author Manuscript

NIH-PA Author Manuscript

NIH-PA Author Manuscript

prototyping give rise to the possibility of designing patient specific implants with complex geometry that can be tailored to the patient's defect site [5]. A scaffold may be used to grow complex tissues such as dentin and pulp when seeded with a suitable cell line [6].

Bone and dental substitution materials should encompass many different characteristics for consideration in clinical use. Not only should the material be porous to serve as a scaffold for capillary growth, the material should have excellent biocompatibility, osteoconductivity, and a complete lack of antigenicity [7]. Ideally, a scaffold will offer mechanical support and will be resorbed as new bone and tissue growth occur. Calcium phosphate (CaP) materials have been widely studied for their use in orthopedic and dental implant applications and tissue scaffolds due to their excellent biocompatibility, controllable bioresorbability and compositional similarity to bone[8-11]. Characteristics of scaffolds such as density, pore shape and size and pore interconnectivity are important parameters that will manipulate tissue ingrowth and mechanical interlocking at the implant-bone interface [12-15]. Many methods for creating complex CaP scaffolds have been investigated including direct and indirect extrusion freeforming, selective laser sintering, stereolithography and ink-jet printing [16]. Direct ink-jet printing has demonstrated very good resolution with great control over the complexity of geometry [17-21]. Other advantages of 3D printing are that macroporosity is induced into the scaffold during the fabrication process without the need for a support structure [22-23]. Moreover, these scaffolds are fabricated directly using the 3D printer with designed materials unlike many other processes where multiple post processing steps are needed.

One of the major disadvantages of ceramic scaffolds is their low strength, especially at high volume percentages of porosity [24]. Recent studies have shown that by doping β-TCP with trace elements commonly found in bone, the dissolution/resorption rates, densification, cell-material interaction and mechanical strength can be controlled [9, 25-29]. One study showed that in osteoporotic subjects, supplemental silicon and monomethyl trisilanol resulted in increases in femoral and lumbar spine bone mass density [30]. The same study demonstrated that this treatment was more effective than a bisphosphonate (Etidronate) and sodium fluoride treatment. Silicon has been proven to be an important trace element in bone and connective tissue formation and can stimulate biological activity by increasing the solubility of the material, generating a more electronegative surface and creating a finer microstructure resulting in transformation of the material surface to a biologically equivalent apatite [31]. Zinc, also an important trace element in bone formation, has been shown to control grain growth, increase density and have stimulatory effects on bone formation when added to CaP [32]. Zinc is released during skeletal breakdown and has been shown to inhibit osteoclastic bone resorption [33]. It does this by inhibiting osteoclast-like cell formation from bone marrow cells and inducing apoptosis of mature osteoclast [34]. Osteoporotic patients have also been shown to have lower levels of skeletal zinc than that of control groups[35]. This study examines the effects of silica (SiO_2) and zinc oxide (ZnO) addition, as a binary dopant system, on the physical, mechanical and biological properties of 3D interconnected porous TCP scaffolds created by the 3-D printing, a solid freeform fabrication method.

2.0 Materials and Methods

2.1 Fabrication of Porous Scaffolds

High purity oxide based sintering additives, silicon dioxide (SiO2) (99%+ purity) and zinc oxide (ZnO) (99.9%+ purity) were purchased from Fisher Scientific (Fair Lawn, NJ). Synthetic β-tricalcium phosphate powder was obtained from Berkley Advanced Biomaterials Inc. (Berkeley, CA) with an average particle size of 550 nm and specific average surface area of 10-50 m^2g^{-1}. Powder was made in batches of 100g and doped with 0.25 wt % ZnO and 0.5 wt % SiO_2 as a binary dopant system. Dopant amounts were chosen

NIH-PA Author Manuscript

NIH-PA Author Manuscript

NIH-PA Author Manuscript

based on previous research from our group [9, 35]. Powder was added to and mixed in 500 mL polypropylene Nalgene bottles, with 300 g of 5 mm diameter zirconia milling media. 150mL of ethanol was added and ball milling was carried out for 6 h at 70 rpm to minimize the formation of agglomerates and increase the homogeneity of the powders. After milling, the Nalgene bottle was placed in an oven at 60° C for 24 h for drying. Milling media were removed and the powder was further dried at 60° C for another 24 h. Finally, agglomerates were removed using a mortar and pestle.

Cylindrical scaffold CAD files (diameter 7 mm and height 10.5 mm) were created with interconnected square channels of 1000μm, 750μm, and 500μm sides **(Fig. 1 (a))**. Scaffolds were fabricated using a 3-D printer (R-1 R&D printer by ProMetal). The printing system consists of a deposition bed that starts with only a small base layer of powder, a feed bed that is filled with powder, a powder spreader, an ink jet print head and a drying unit. A schematic representation of operation is given in **Figure 1 (b)**. The printer head sprays binder onto the loose powder in the deposition bed according to the CAD pattern, the deposition bed is lowered by 20 μm and the feeder bed is raised by 60 μm. The spreader will then push the excess powder from the feeder bed and evenly spread it onto the lowered deposition bed. The process is repeated, layer by layer, until the CAD image is completely printed. Parts were built in 20μm layers thickness with commercial organic water based binder obtained from ProMetal (Irwin, Pa). Once finished, parts were dried at 150°C for 1.5 h. Green scaffolds were then gently brushed clean and the remaining powder was removed by using a compressed air blower. After cleaning, green scaffolds were sintered in a muffle furnace at 1250° C for 2 h. Important fabrication parameters that were optimized include binder selection, binder drop size and amount deposited, powder particle size, drying time between layers, powder spread rate, build layer thickness and powder feed to build ratio.

2.2 Microstructure, Phase Analysis and Mechanical Properties

The surface morphologies of the sintered scaffolds were observed under a field emission scanning electron microscope (FESEM) (FEI Inc., OR, USA). Phase analysis of sintered β-TCP samples with and without dopants was carried out by X-ray diffraction (XRD) using a Siemens D-500 X-ray powder Diffractometer (Siemens AG, Karlsruhe, Germany) with CuK_{α} radiation and a Ni-filter. Each run was performed with 2θ values between 10° and 60° at a step size of 0.02° and a count time of 0.5 s per step. Density was measured using Archimedes method. Samples were weighed initially dry and then submerged in boiling water for 3 minutes to remove any excess air that may be trapped in the porous structure. The samples were then transferred from the boiling water to room temperature water, where the weight was recorded again (n=3). Compressive strengths of undoped and doped TCP scaffolds were determined using a screw-driven universal testing machine (AG-IS, Shimadzu, Japan) with a constant crosshead speed of 0.33 mm/min. Compressive strength was calculated using the maximum load recorded and the sample dimensions. Compressive strength was tested on ten samples for each composition.

2.3 *In Vitro* Osteoblast Cell-Material Interactions

Pure and doped TCP samples were studied for their cell-materials interactions using established human fetal osteoblast (hFOB) cells (hFOB 1.19, ATCC, Manassas, VA). The base medium for this cell line was a 1:1 mixture of Ham's F12 Medium and Dulbecco's Modified Eagle's Medium (DMEM/F12, Sigma, St. Louis, MO), with 2.5 mM L-glutamine (without phenol red). This base medium was supplemented with 10% fetal bovine serum (HyClone, Logan, UT) and 0.3 mg/mL G418 (Sigma, St. Louis, MO).

All scaffolds were sterilized by autoclaving at 121°C for 30 min and then placed in 24-well plates. Cells were then seeded onto the samples. Cultures were maintained at 34°C under a

NIH-PA Author Manuscript

NIH-PA Author Manuscript

NIH-PA Author Manuscript

5% CO_2 atmosphere as recommended by ATCC for hFOB 1.19. The medium was changed every 2 to 3 days for the duration of the experiment.

An MTT (3-(4,5-dimethylthiazol-2-yl)-2,5-diphenyl tetrazolium bromide) assay was used to evaluate cell proliferation. The MTT (Sigma, St. Louis, MO) solution of 5 mg/ml was prepared by dissolving MTT in PBS and the solution then filter-sterilized (0.2 μm). The MTT was diluted (100 μL into 900 μL) in DMEM/F12 medium and 1 mL of the diluted solution was then added to each of the samples. After 2 h of incubation, 1 mL of solubilization solution made up of 10% Triton X-100, 0.1N HCl, and isopropanol was added to dissolve the formazan crystals. 100 μL of the resulting supernatant was transferred into a 96-well plate, and read by a plate reader at 570 nm. Cultures were evaluated at 3, 7 and 11 days. Data was normalized to pure TCP control scaffolds with corresponding pore parameters.

Samples for SEM observation were collected at days 3, 7 and 11 and fixed with 2% paraformaldehyde/2% glutaraldehyde in 0.1M cacodylate buffer overnight at 4 °C. Post-fixation was performed with 2% osmium tetroxide (OsO4) for 2 hours at room temperature. Fixed samples were then dehydrated in an ethanol series (30%, 50%, 70%, 95% and 100% three times), followed by a hexamethyldisilane (HMDS) drying procedure. After gold sputtering, samples were observed under FESEM.

3.0 Results

3.1 Scaffold Fabrication

The Ex One R1 3D printer was commercially designed and optimized for the use of metal powders. Our goal in this study was to produce scaffolds using CaP ceramic powders. One of the major challenges was the optimization of processing parameters to effectively produce these scaffolds using commercially available binder. Our process optimization research approach was first focused on how to produce a green TCP part followed by how to improve green strength of the part for mechanical handleability and depowderization to produce a 3D interconnected porous scaffold. Processing parameters used are given in **Table 1**. The drop volume is a fixed parameter that is measured by the printer and is dictated by the viscosity and density of the binder. It is a measurement of the volume of each drop of binder that is released from a nozzle on the print head. The drop volume measured for the commercial binder used was 76 pL. The saturation percentage is based on the drop volume, packing efficiency of the powder layer and binder viscosity. The 100% value is a good starting point to work with because it is essentially a calculated estimate of how the binder will spread through the powder. If the saturation is too high, the binder will bleed into the surrounding powder, while too little saturation will result in extremely weak green scaffolds due to poor bonding between layers. The values that worked best were 110% for pure TCP powder and 100% for doped TCP powder. The pure TCP needed a little extra binder to maintain strength while handling and depowdering. The number of passes that the print head used to reach the desired saturation was 7 at a speed of 140 mm/s. The layer thickness was an important parameter because it dictated the depth resolution of the scaffold. The primary concern that was taken into consideration when choosing a layer thickness was the size of the powder particles. By using very fine powder, 550 nm, layer thicknesses of 20 μm for pure TCP powder and 30 μm for doped TCP powder were achieved while maintaining very smooth spreading. The doped powder had less depth resolution due to slight agglomeration of particles during the ball milling process. The feed powder to layer thickness ratio chosen was 3. This means that for every 20 or 30 μm that the build bed is lowered, the feed bed is raised by 60 or 90 μm, respectively. To help ensure that the powder is spread smoothly onto the build bed, a spread speed of 0.5 mm/s was used. This is the speed that the beds pass under the rolling spreader. As the beds move, loose powder from the raised feed layer is

NIH-PA Author Manuscript

NIH-PA Author Manuscript

NIH-PA Author Manuscript

spread evenly onto the lowered build layer. By understanding the fixed processing parameters and using this information to adjust the variable processing parameters, we were able to successfully produce high resolution scaffolds with both doped and pure TCP powders.

3.2 Physical and Mechanical Characterization

XRD was performed to determine the CaP phases of the sintered scaffolds and confirmed that in both samples, β-TCP was the primary phase present after sintering at 1250 °C. α-TCP phase was also present in small amounts in both samples, which is expected at sintering temperatures above 1150 °C. The amount of α phase present in the doped samples was smaller than in the pure composition as shown in **Figure 2**. The characteristic peaks of β-TCP and α-TCP match well with JCPDS # 09-0169 (β-TCP) and 09-0348 (α-TCP), but show a small peak shift in the doped TCP samples. Such peak shifts due to dopant addition are common and reported by other researchers as well.

Density and designed percent porosity for sintered scaffolds are shown in **Table 2.** The average apparent strut density of the SiO_2/ZnO doped scaffolds was found to be 94.1 ± 1.6% and for pure TCP scaffolds strut density was measured to be 90.8 ± 0.8%. **Figure 3** shows the surface morphology of samples sintered at 1250 °C. The microstructures of both pure and doped scaffolds showed some residual porosity, 9% and 5% by volume, respectively. Both samples also showed evidence of liquid phase sintering. **Table 3** gives data collected from these micrographs, demonstrating that there was more shrinkage in the doped samples than in their pure counterparts. Compressive strength comparisons between doped and pure scaffolds are presented in **Figure 4**. The doped samples, which had less total open pore volume than the pure samples, showed the greatest compressive strength with 1000μm, 750μm and 500μm green channel sizes at 10.21 ± 0.11 MPa, 8.2 ± 0.4 MPa and 4.34 ± 0.3 MPa, respectively. The pure samples with green channel sizes 1000μm, 750μm and 500μm had average compressive strengths of 5.48 ± 0.04 MPa, 2.68 ± 0.2 MPa and 1.75 ± 0.2 MPa, respectively.

3.3 *In Vitro* Biological Characterization

MTT results depict a clear distinction between the SiO_2/ZnO doped scaffolds and the pure TCP control scaffolds, given in **Figure 5**. The amount of viable cells was significantly greater in the doped samples than on the pure scaffolds. Data ranged from a 3% increase as a low on day 3, to 92% more viable cells as a high on day 11. SEM micrographs confirmed data gathered from the MTT assay. The micrographs show on day 3 that cellular attachment characteristics were good in both doped and pure scaffolds, with osteoblast cells extending and attaching to various anchor points. By day 7, there was a clear proliferation distinction between the doped and pure samples, with doped samples exhibiting significantly larger groups of cells attaching to the surface. In both cases, complex filipodial communication networks were beginning to emerge between nearby cells, as shown in **Figure 6.**

4.0 Discussion

One of the major challenges of this study was the optimization of the processing parameters of the 3D printer to produce high quality scaffolds. While there are several factors that need to be taken into consideration, as mentioned previously, the ability to create conditions that result in uniform and smooth powder spreading and high green strength are what made this study successful. A smooth powder build layer is extremely important to the mechanical strength of the scaffolds. If the build layer is rough, defects are incorporated into the structure during the printing process resulting in decreased mechanical strength of sintered scaffolds as well as diminished ability to handle greens scaffolds. Binder choice was also an

NIH-PA Author Manuscript

NIH-PA Author Manuscript

NIH-PA Author Manuscript

important factor. The binder had to fluid enough to penetrate through the powder build layer to give good bonding between layers, but viscous enough that it did not bleed into areas surrounding the print pattern. Also, due to complex geometry, it had to offer enough mechanical support to withstand the vigorous cleaning and depowdering process to ensure interconnectivity between the pores in the scaffolds.

Present results show that addition of SiO_2 and ZnO to 3-D interconnected porous TCP scaffolds can influence both biological and mechanical properties of the scaffolds. Sintering additives have been investigated in the past for dense and porous TCP and hydroxyapatite compacts to increase the density and mechanical strength [35-36], however there have been no studies examining the effects on 3D printed scaffolds. XRD patterns shown in **Figure 2** confirm that the α-TCP phase formation is reduced in the SiO_2/ZnO doped samples when compared to pure TCP scaffolds sintered at the same temperature and time. In the case of TCP ceramics, dopants are used as a sintering additive to retard the transformation of β-TCP to α-TCP at temperatures above 1150 °C. Studies have indicated that the presence of α-phase is closely related with the expansion of sample volume, declining shrinkage rate and is generally considered to prevent TCP from further densification [37-38]. Both compositions also showed evidence of some liquid-phase sintering, demonstrated in **Figure 3**, which is beneficial because it results in a more uniform densification than that of solid state sintering. Channel size analysis, given in **Table 2**, in sintered samples demonstrates overall volume shrinkage. When compared to pure TCP scaffolds, the doped samples revealed increased density, specified in **Table 1**, which can be attributed to reduced α-TCP formation.Another possible mechanism of increased densification would be enhanced wettability during liquid-phase sintering in the doped samples. Greater wettability during sintering would lead to more efficient capillary action and particle rearrangement. Ultimately, density and designed porosity play the most important role to increase the maximum strength of the samples [24]. Pores act as stress concentrators and may lead to premature failure if in the near vicinity of other defects such as inclusions, agglomerates and surface flaws. The average compressive strength for the doped scaffolds was higher than their pure counterparts with a mean 250% increase in strength for each channel size. The pure scaffolds matched well with the lower end strength of cancellous bone, while the doped scaffolds matched well with the higher end strength of cancellous bone, which has a strength range of 0.5 – 14.6 MPa. These results indicate that with the addition of dopants, TCP scaffolds may be tailored to match specific strength criteria for a given application. TCP resorption rates and strength degradation may also be tailored by the addition dopants [39,40]. Previous studies have shown that the presence of zinc and silicon increase the rate of mineralization in simulated body fluid [9,41,42]. Where silicon and zinc may act as nucleation sites or create conditions that are favorable for apatite formation and at the same time slowing the dissolution process *in vitro* [43]. The dissolution properties of the scaffold can be affected by density, grain size and grain uniformity as well as the overall macrostructure porosity.

Additional issues to be considered when evaluating the performance of a viable scaffold for clinical applications are the initial fixation period and healing time after a surgical procedure. While CaP materials alone are excellent for bone replacement applications, there is merit in investigating the use of dopants to enhance proliferation and differentiation of bone building osteoblasts. MTT data shows that cells proliferate at a greater rate within the doped samples when compared a pure TCP control group as seen in **Figure 5**. SEM micrographs taken of hFOB cells seeded and incubated on the scaffolds, presented in **Figure 6**, show similar cellular morphology between the doped and pure scaffolds. At day 3, the cells are elongated and flattened and are growing into the abundance of micropores. By day 7, complex filipodial communication networks are set up between neighboring cells and there is a clear increase in the amount of living cells on the surface of the doped scaffolds when compared to the pure TCP scaffolds. Zinc plays an important role in bone metabolism,

NIH-PA Author Manuscript

NIH-PA Author Manuscript

NIH-PA Author Manuscript

where deficiency may result in bone loss. Studies have shown that zinc has a stimulatory effect on bone formation *in vitro* and *in vivo* and increases alkaline phosphatase activity, an enzymatic marker for osteoblastic differentiation [44-45]. Studies have demonstrated that addition of zinc as a dopant to CaP ceramics resulted in a significantly greater amount of new bone formation *in vivo* when compared the pure composition [46]. Zinc dopants in TCP/HA binary compositions have also been shown to increase the osteoblastic differentiation from bone marrow stromal cells *in vitro* [47]. While the mechanisms of action are not yet fully realized, recent studies have begun to consider the cellular response in more detail. One investigation reported that zinc had a direct effect on osteoclast precursor cells by reducing receptor for activation of NF-κB (RANK) expression [48]. Osteoclastic differentiation occurs when receptor for activation of NF-κB ligand (RANKL) binds to its receptor RANK and activates NF-κB and activator protein-1 (AP-1). A similar observation confirmed the results showing a significant repression of basal NF-κB activity in preosteoclast cells *in-vitro* and also showed significant reduction in tumor necrosis factor-alpha (TNFα) and stimulation of osteoblast mineralization [49]. TNFα is an osteoclastogenic cytokine present in osteoblasts that not only upregulates production of RANKL but also coordinates with it to intensify its osteoclastogenic activity [50-52]. It has also been shown that zinc plays a critical role in the production and release of vascular endothelial growth factor (VEGF) by osteoblasts [53]. VEGF stimulates the proliferation of vascular endothelial cells which, during bone remodeling, provide microvasculature.

Increased silicon dietary uptake has been linked to better bone health and increased bone mineral density while lab studies have shown positive effects on osteoblast proliferation and differentiation [54-55]. *In vivo* research has shown increased bone regeneration from silicon doped CaP materials when compared to their pure counterparts [56-57]. Other investigations have shown materials doped with silicon stimulate alkaline phosphatase activity in osteoblasts and mesenchymal stem cells [58]. A recent study found that silica-CaP composites lead osteoblasts to rapid advancement to the differentiation stage indicated by increased osteopontin and osteocalcin mRNA expression[59]. Another group found that with the addition of silica to cell media increased collagen type 1 (COL1) gene expression and extracellular signal regulated kinases (ERK) secretion [60]. COL 1 is known to play a role in angiogenesis and can regulate proliferation, differentiation, migration, and morphogenesis. ERK is a member of the mitogen-activated protein kinase (MAPK) family of protein kinases involved in the proliferation, differentiation, and apoptosis of bone cells [61]. Present results suggest that the addition of dopants to TCP scaffolds can have a significant effect on cellular behavior. This is likely due to the dissolution of the scaffold and subsequent release of Zn^{2+} and Si^{4+} ions into the media. Further studies are required to fully understand this mechanism.

The effects of designed macropore size on tissue-material interaction would best be determined in an animal model. For such a study it would be important to consider the performance tradeoffs in tissue integration vs. mechanical strength. There is enough compelling evidence that SiO_2/ZnO doped scaffolds perform better, mechanically and biologically, than pure TCP scaffolds to justify *in vivo* studies in the future. 3D printing is shown to be a viable manufacturing tool for tailored porosity TCP scaffolds with and without dopants for future clinical studies and applications in dental and orthopedic applications.

Conclusion

The present study examined the influence of a SiO_2/ZnO binary dopant system on the mechanical and biological properties of designed macroporous TCP scaffolds fabricated using commercial 3D printing technology. The addition of dopants decreased the β to α

NIH-PA Author Manuscript

NIH-PA Author Manuscript

NIH-PA Author Manuscript

phase transformation of TCP sintered at 1250 °C, increased densification and as a result, showed up to 250% increase in compressive strength when compared to pure TCP scaffolds. A maximum compressive strength of 10.21 ± 0.33 MPa was achieved in doped scaffolds with 500 μm interconnected macropores. MTT assay and SEM analysis of cellular interaction suggests that the doped samples increased cellular attachment and proliferation. These results establish SiO_2/ZnO doped TCP scaffolds with interconnected channels fabricated via 3D printing as viable candidates for further research in clinical applications in non-load bearing bone tissue replacements.

Acknowledgments

Authors would like to acknowledge financial support from the National Institutes of Health, NIBIB (Grant # NIH-R01-EB-007351).

7.0 References

1. Zheng L, Yang F, Shen H, Hu X, Mochizuki C, Sato M, Wang S, Zhang. The effect of composition of calcium phosphate composite scaffolds on the formation of tooth tissue from human dental pulp stem cells. Biomaterials. 2011; 32:7053–59. [PubMed: 21722953]
2. Wang J, Liu X, Jin X, Ma H, Hu J, Ni L, Ma PX. The odontogenic differentiation of human dental pulp stem cells on nanofibrous poly(L-lactic acid) scaffolds *in vitro* and *in vivo*. Acta Biomaterialia. 2010; 6:3856–63. [PubMed: 20406702]
3. Dietschi D, Duc O, Krejci I, Sadan A. Biomechanical considerations for the restoration of endodontically treated teeth: a systematic review of the literature—Part I. Composition and micro- and macrostructure alterations. Quintessence Int. 2007; 38:733. [PubMed: 17873980]
4. Dietschi D, Duc O, Krejci I, Sadan A. Biomechanical considerations for the restoration of endodontically treated teeth: a systematic review of the literature—Part II. Evaluation of fatigue behavior, interfaces, and *in vivo* studies. Quintessence Int. 2008; 39:117. [PubMed: 18560650]
5. Darsell J, Bose S, Hosick H, Bandyopadhyay A. "From CT Scans to Ceramic Bone Grafts. Journal of the American Ceramic Society. 2003; 86:1076–80.
6. Wang J, Ma H, Jin X, Hu J, Liu X, Ni L, Ma. The effect of scaffold architecture on odontogenic differentiation of human dental pulp stem cells. Biomaterials. 2011; 32:7822–7830. [PubMed: 21663962]
7. Neamat A, Gawish A, Gamal-Eldeen AM. B-Tricalcium phosphate promotes cell proliferation, osteogenesis and bone regeneration in intrabony defects in dogs. Archives of Oral Biology. 2009; 54:1083–90. [PubMed: 19828137]
8. Enderlea R, Gotz-Neunhoeffera F, Gobbelsa M, Mullerb FA, Greilb P. Influence of magnesium doping on the phase transformation temperature of b-TCP ceramics examined by Rietveld refinement. Biomaterials. 2005; 26:3379–84. [PubMed: 15621226]
9. Bandyopadhyay A, Bernard S, Xue W, Bose S. Calcium Phosphate-Based Resorbable Ceramics: Influence of MgO, ZnO, and SiO2 Dopants. J. Am. Ceram. Soc. 2006; 89:2675–88.
10. Bandyopadhyay, A.; Bose, S. Materials and Design of Orthopedic Devices.. In: Wiley, J., editor. Encyclopedia of Medical Devices and Instrumentation . 2nd ed.. John Wiley & Sons; Chichester: 2006. p. 187-92.
11. Kondo N, Ogose A, Tokunaga K, Ito T, Arai K, Kudo N. Bone formation and resorption of highly purified B-tricalcium phosphate in the rat femoral condyle. Biomaterials. 2005; 26:5600–08. [PubMed: 15878364]
12. Hulbert SF, Young FA, Mathews RS, Klawitter JJ, Talbert CD, Stelling FH. Potential of ceramic materials as permanently implantable skeletal prostheses. J. Biomed. Mater. Res. 1970; 4:433. [PubMed: 5469185]
13. Hui PW, Leung PC, Sher A. Fluid conductance of cancellous bone graft as a predictor for graft-host interface healing. J Biomech. 1996; 29:123–32. [PubMed: 8839025]

NIH-PA Author Manuscript

NIH-PA Author Manuscript

NIH-PA Author Manuscript

14. Kuboki Y, Jin Q, Takita H. Geometry of carriers controlling phenotypic expression in BMP induced osteogenesis and chondrogenesis. J Bone Joint Surg Am (Suppl. 2001; 1(Pt 2):S105–S115.
15. Bose S, Suguira S, Bandyopadhyay A. Processing of controlled porosity ceramic structures. Scripta Materialia. 1999; 41:1009–14.
16. Hollister SJ. Porous scaffold design in tissue engineering. Nature Materials. 2005; 4:518–24.
17. Franco J, Hunger P, Launey ME, Tomsia AP, Saiz E. Direct write assembly of calcium phosphate scaffolds using a water-based hydrogel. Acta Biomaterialia. 2010; 6:218–28. [PubMed: 19563923]
18. Vorndran E, Klammert U, Klarner M, Grover LM, Barralet JE, Gbureck U. 3D printing of β-tricalcium phosphate ceramics. Dental Materials. 2009; 25:e18–e19.
19. Khalyfa A, Vogt S, Weisser J, Grimm G, Rechtenbach A, Meyer W, Schnabelrauch M. Development of a new calcium phosphate powder-binder system for the 3D printing of patient specific implants. J Mater Sci: Mater med. 2007; 18:909–16. [PubMed: 17216579]
20. Becker S, Bolte H, Krapf O, Seitz H, Douglas T, Sivananthan S, Wiltfang J, Sherry E, Warnke P. Endocultivation: 3D Printed customized poroous scaffolds for heterotopic bone induction. Oral Oncololgy. 2009; 45:e181–e188.
21. Z. Ahmad ES, Thian J, Huang MJ, Edirisinghe SN, Jayasinghe DC, Ireland RA, et al. Freeform Fabrication of Nano-biomaterials using 3D Electrohydrodynamic Print-patterning. J.Biomed. Nanotech. 2008; 4:185–95.
22. Habibovic P, Gbureck U, Doillon C, Bassett D, Blitterswijk C, Barralet J. Osteoconduction and osteoinduction of low-temperature 3D printed bioceramic implants. Biomaterials. 2008; 29:944–953. [PubMed: 18055009]
23. Bergmann C, Linder M, Zhang W, Koczur K, Kirsten A, Telle R, Fischer H. 3D printing of bone substitute implants using calcium phosphate and bioactive glasses. Journal of the European Ceramic Society. 2010; 30:2563–67.
24. Bose S, Darsell J, Kintner M, Hosick H, Bandyopadhyay A. Pore Size and Pore Volume Effects on Calcium Phosphate Based Ceramics. Materials Science and Engineering C. 2003; 23:479–86.
25. Kalita S, Bose S, Hosick HL, Bandyopadhyay A. CaO-P2O5-Na2O based sintering additives for hydroxyapatite (HAp) ceramics. Biomaterials. 2004; 25:2332–39.
26. Hattiangadi A, Bandyopadhyay A. Strength Degradation of Porous Ceramics Under Uniaxial Compressive Loading. Journal of the American Ceramic Society. 2000; 83:2730–36.
27. Pietak AM, Reid JW, Stott MJ, Sayer M. Silicon substitution in the calcium phosphate bioceramics. Biomaterials. 2007; 28:4023–32. [PubMed: 17544500]
28. Seeley Z, Bandyopadhyay A, Bose S. Tricalcium phosphate based resorbable ceramics: Influence of NaF and CaO addition. Materials Science & Engineering C - Biomimetic and Supramolecular Systems. 2008; 28:11–17.
29. Seeley Z, Bandyopadhyay A, Bose S. Influence of TiO2 and Ag2O addition on tricalcium phosphate ceramics. J. Biomed. Mater. Res. 2007; 82A:113–21.
30. Eisinger J, Clairet D. Effects of silicon, fluoride, etidronate and magnesium on bone mineral density: a retrospective study. Magnesium Research. 1993; 6:247–249. [PubMed: 8292498]
31. Pietak A, Reid J, Stott M, Sayer M. Silicon substitution in the calcium phosphate bioceramics. Biomaterials. 2007; 28:4023–32. [PubMed: 17544500]
32. Porter AE, Patel N, Skepper JN, Best SM, Bonfield W. Effect of sintered silicatesubstituted hydroxyapatite on remodelling processes at the bone–implant interface. Biomaterials. 2004; 25:3303–14. [PubMed: 14980425]
33. Yamaguchi M. Role of nutritional zinc in the prevention of osteoporosis. Mol. Cell. Biochem. 2010; 338:241–54. [PubMed: 20035439]
34. Murray EJ, Messer HH. Turnover of bone zinc during normal and accelerated bone loss in rats. J Nutr. 1981; 111:1641–1647. [PubMed: 7277041]
35. Reginster JY, Strause LG, Saltman O, Franchimont P. Trace elements and postmenopausal osteoporosis: a preliminary study of decreased serum manganese. Med Sci Res. 1988; 16:337–338.

NIH-PA Author Manuscript

NIH-PA Author Manuscript

NIH-PA Author Manuscript

36. Xue W, Dahlquist K, Banerjee A, Bandyopadhyay A, Bose S. Synthesis and characterization of tricalcium phosphate with Zn and Mg based dopants. J Mater Sci: Mater Med. 2008; 19:2669–77. [PubMed: 18270806]
37. Suchanek W, Yashima M, Kakihana M, Yohimura M. Hydroxyapatite ceramics with selected sinting additives. Biomaterials. 1997; 18:923–33. [PubMed: 9199762]
38. Kanazawa T, Umegaki T, Yamashita K, Monma H, Hiramatsu T. The effecs of additives on sintering and some properties of calcium phosphates with various Ca/P ratios. J. Mater. Sci. 1991; 26:417–22.
39. Bose S, Tarafder S, Banerjee S, Davies NM. Understanding *in vivo* response and mechanical property variation in MgO, SrO and SiO_2 doped β-TCP. Bone. 2011; 48:1282–90. [PubMed: 21419884]
40. Banerjee S, Tarafder S, Davies NM, Bandyopadhyay A, Bose S. Understanding the influence of MgO and SrO binary doping on the mechanical and biological properties of β-TCP ceramics. Acta Biomaterialia. 2010; 6:4167–74. [PubMed: 20493283]
41. Ryu HS, Youn HJ, Hon KS, Chang BS, Lee CK, Chung SS. An improvement of sintering property of B-tricalcium phosphate by addition of calcium pyrophosphate. Biomaterials. 2002; 23:909–14. [PubMed: 11771710]
42. Canham LT, Reeves CL, Loni A, Houlton MR, Newey JP, Simons AJ. Cox. Calcium phosphate nucleation on porous silicon: factors influencing kinetics in acellular simulated body fluids. Thin Solid Films. 1997; 297:304–7.
43. Wei X, Ugurlu O, Ankit A, Acar HY, Akinc M. Dissolution behavior of Si,Zn-codoped tricalcium phosphates. Materials Science and Engineering C. 2009; 29:126–35.
44. Hashizume M, Yamaguchi M. Effect of beta-alanyl-L-histidinato zinc on differentiation of osteoblastic MC3T3-E1 cells: increases in alkaline phosphatase activity and protein concentration. Molecular and Cellular Biochemistry. 1994; 131:19–24. [PubMed: 8047061]
45. Yamaguchi M, Yamaguchi R. Action of zinc on bone metabolism in rats. Increases in alkaline phosphatase activity and DNA content. Biochemical Pharmacology. 1986; 35:773–77. [PubMed: 3954786]
46. Xia L, Sogo Y, Ito A, Mutsuzaki H, Ochiai N, Kobayashi T, Nakamura S, Yamashita K, LeGeros RZ. The optimum zinc content in set calcium phosphate cement for promoting bone formation *in vivo*. Materials Science and Engineering C. 2009; 29:969–75. [PubMed: 21461346]
47. Ito A, Kawamura H, Otsuka M, Ikeuchi M, Ohgushi H, Ishikawa K, Onuma K, Kanzaki N, Sogo Y, Ichinose N. Zinc-releasing calcium phosphate for stimulating bone formation. Materials Science and Engineering C. 2002; 22:21–5.
48. Hie M, Tsukamoto I. Administration of zinc inhibits osteoclastogenesis through the suppression of RANK expression in bone. Molecular and Cellular Pharmacology. 668:140–46. 201.
59. Yamaguchi M, Weitzmann N. Zinc stimulates osteoblastogenesis and suppresses osteoclastogenesis by antagonizing NF-κB activation. Mol Cell Biochem. 2011; 355:179–86. [PubMed: 21533765]
50. Cenci S, Weitzmann MN, Roggia C, Namba N, Novack D, Woodring J. Estrogen deficiency induces bone loss by enhancing T-cell production of TNF-alpha. J Clin Invest. 2000; 106:1229–1237. [PubMed: 11086024]
51. Lam J, Takeshita S, Barker JE, Kanagawa O, Ross FP, Teitelbaum SL. TNF-alpha induces osteoclastogenesis by direct stimulation of macrophages exposed to permissive levels of RANK ligand. J Clin Invest. 2000; 106:1481–1488. [PubMed: 11120755]
52. Zhang YH, Heulsmann A, Tondravi MM, Mukherjee A, Abu-Amer Y. Tumor necrosis factor-alpha (TNF) stimulates RANKL-induced osteoclastogenesis via coupling of TNF type 1receptor and RANK signaling pathways. J Biol Chem. 2001; 276:563–568. [PubMed: 11032840]
53. Hanai Y, Tokuda H, Yasuda E, Noda T, Ohta T, Takai S, Kozawa O. Up-regulation by zinc of FGF-2-induced VEGF release through enhancing p44/p42 MAP kinase activation in osteoblasts. Life Sciences. 2006; 80:230–34. [PubMed: 17020773]
54. Jugdaosingh R. Silicon and Bone Health. J Nutr Health Aging. 2007; 11:99–110. [PubMed: 17435952]

NIH-PA Author Manuscript

NIH-PA Author Manuscript

NIH-PA Author Manuscript

55. Thian ES, Huang J, Best SM, Barber ZH, Brooks RA, Rushton N, et al. The response of osteoblasts to nanocrystalline silicon-substituted hydroxyapatite thin films. Biomaterials. 2006; 27:2692–8. [PubMed: 16423389]

56. Patel N, Brooks RA, Clarke MT, Lee PMT, Rushton M, Gibson IR, Best SM, Bonfield W. *In vivo* assessment of hydroxyapatite and silicate-substituted hydroxyapatite granules using an ovine defect model. Journal of Materials Science: Materials in Medicine. 2005; 16:429–40. [PubMed: 15875253]

57. Camire C, Jegou Saint-Jean S, Mochales C, Nevsten P. Wang JS, Lidgren L, McCarthy I, Ginebra MP. Material Characterization and *In Vivo* Behavior of Silicon Substituted α-Tricalcium Phosphate Cement. JBMR B. 2006; 76:241–68.

58. Obata A, Kasuga T. Stimulation of human mesenchymal stem cells and osteoblasts activities *in vitro* on silicon-releasable scaffolds. JBMR A. 2009; 91:11–17.

59. Gupta G, Kirakodu S, Ghannam A. Effects of exogenous phosphorus and silicon on osteoblast differentiation at the interface with bioactive ceramics. JBMR A. 2010; 95:882–90.

60. Shie MY, Ding SJ, Chang HC. The role of silicon in osteoblast-like cell proliferation and apoptosis. Acta Biomaterialia. 2011; 7:2604–2614. [PubMed: 21345382]

61. Huang Z, Cheng SL, Slatopolsky E. Sustained activation of the extracellular signal-regulated kinase pathway is required for extracellular calcium stimulation of human osteoblast proliferation. J Biol Chem. 2001; 276:21351–8. [PubMed: 11292824]

NIH-PA Author Manuscript

NIH-PA Author Manuscript

NIH-PA Author Manuscript

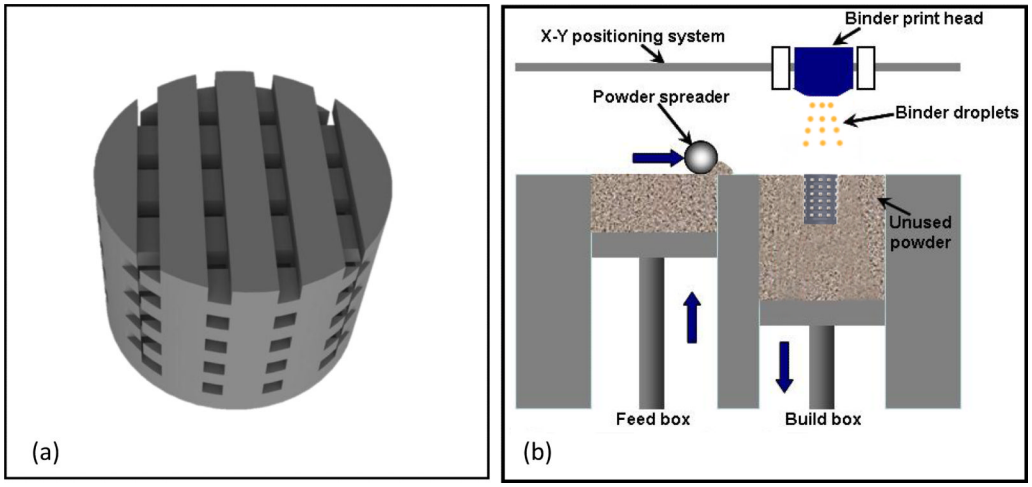

Figure 1.
(a) CAD image of a cross section of a porous scaffold. Square channels are oriented 0°/90° for subsequent layers. (b) Schematic drawing representing the 3D printing process.

NIH-PA Author Manuscript
NIH-PA Author Manuscript
NIH-PA Author Manuscript

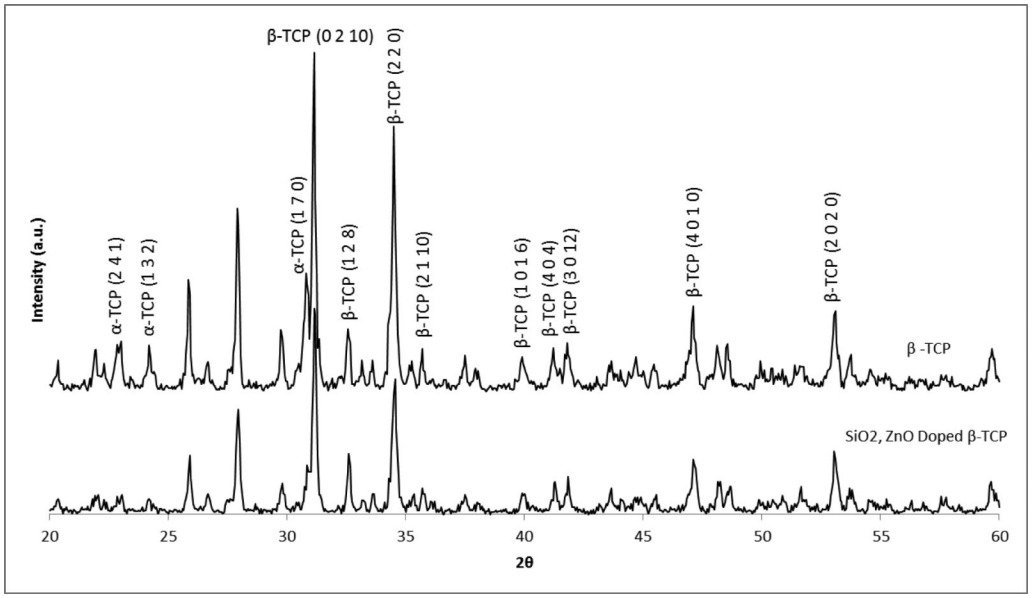

Figure 2.
XRD patterns of doped and pure scaffolds sintered at 1250 °C. JCPDS # 09-0169 (β-TCP) and 09-0348 (α-TCP)

NIH-PA Author Manuscript
NIH-PA Author Manuscript
NIH-PA Author Manuscript

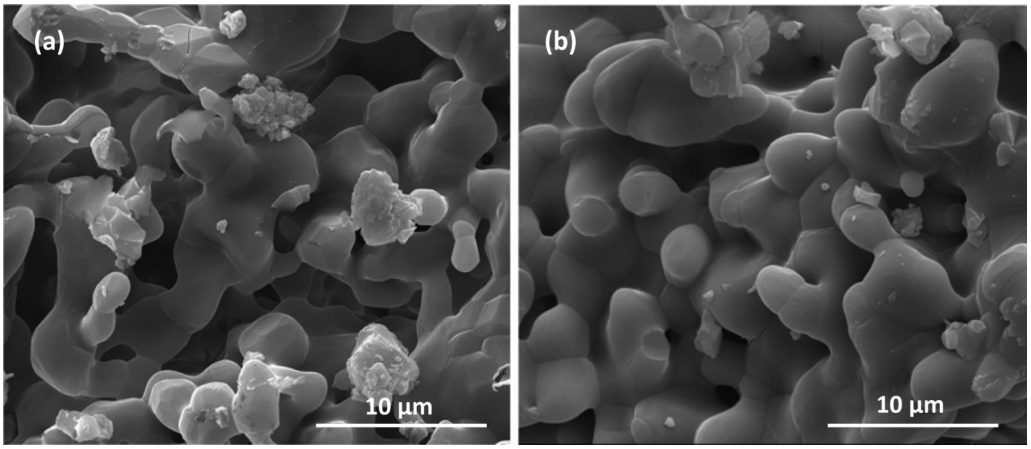

Figure 3.
Surface morphology of sintered scaffolds of (a) pure TCP composition and (b) SiO_2/ZnO doped composition.

NIH-PA Author Manuscript

NIH-PA Author Manuscript

NIH-PA Author Manuscript

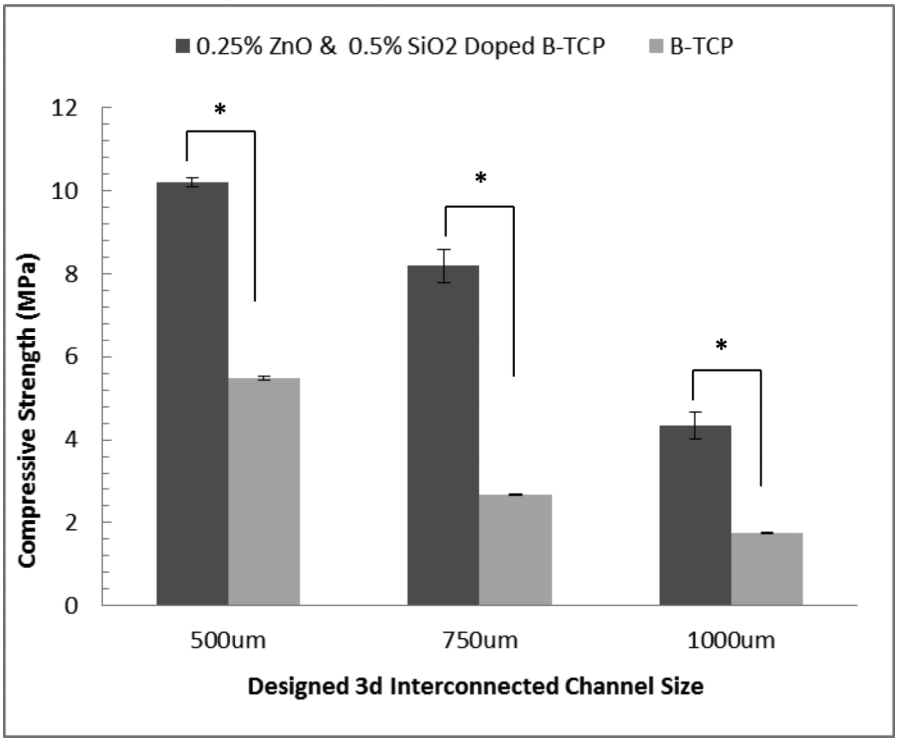

Figure 4.
Compressive strengths of sintered 3D printed scaffolds for both pure and doped β-TCP. Statistical analysis shows that the differences are significant (* $P << 0.05$, where $n = 10$)

NIH-PA Author Manuscript

NIH-PA Author Manuscript

NIH-PA Author Manuscript

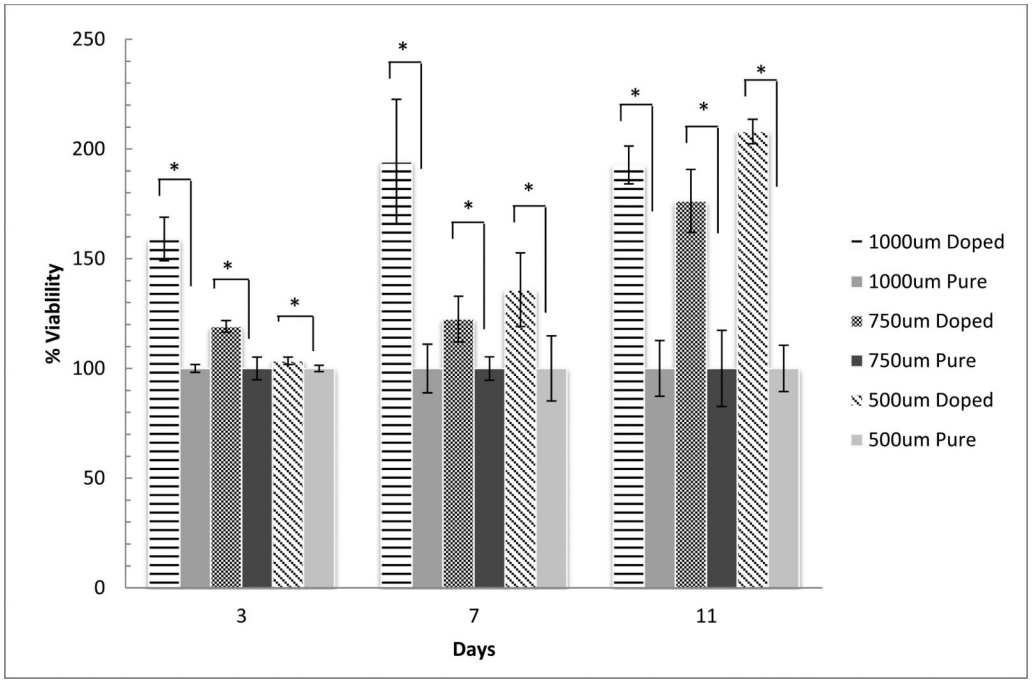

Figure 5.
MTT assay of hFOB on TCP scaffolds with 500 μm, 750 μm, and 1000 μm 3D interconnected channels after 3, 7, and 11 days. Data is normalized to the pure TCP controls for each channel size and day point. (*$p < 0.05$, $n = 3$)

NIH-PA Author Manuscript

NIH-PA Author Manuscript

NIH-PA Author Manuscript

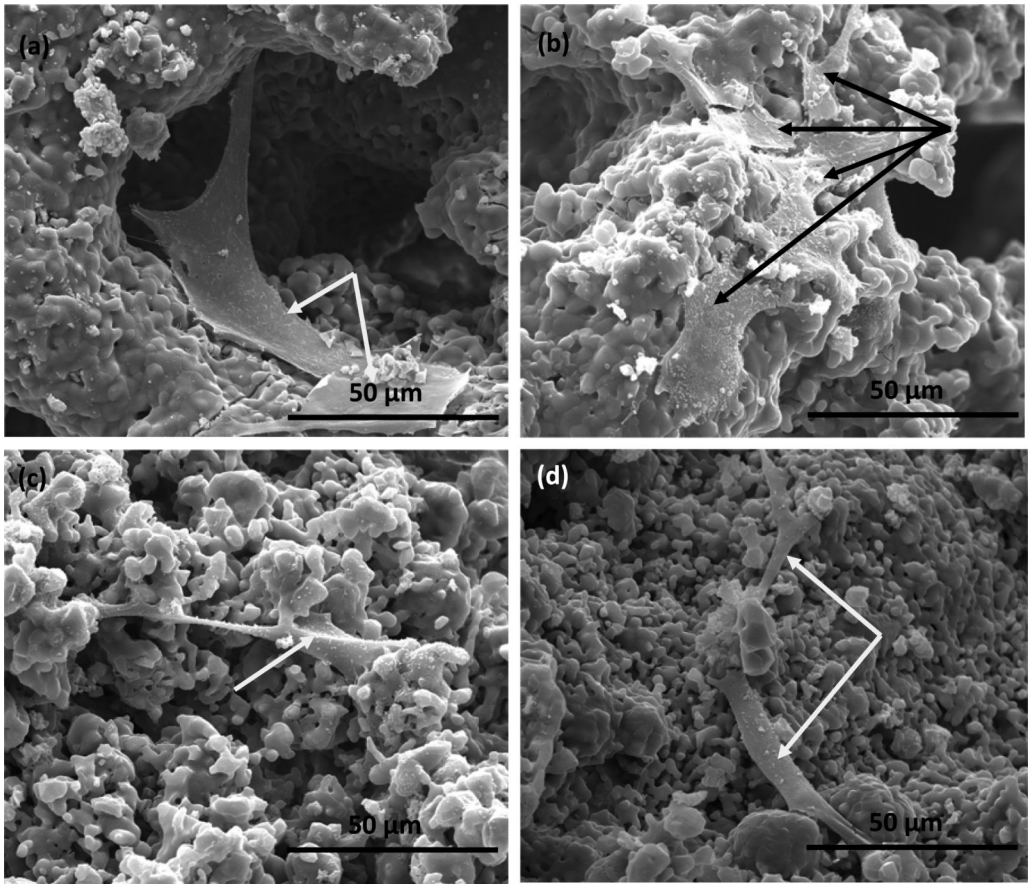

Figure 6.
SEM micrographs of hFOB cells showing the cell adhesion morphology on the scaffold surface and inside the 3D interconnected macropores: (a) doped TCP at 3 days, (b) doped TCP at 7 days, (c) pure TCP at 3 days, (d) pure TCP at 7 days. Arrows are indicating hFOB cells.

NIH-PA Author Manuscript

NIH-PA Author Manuscript

NIH-PA Author Manuscript

Table 1

A list of important 3D printing parameters for fabrication of CaP scaffolds.

Processing Parameters	Pure TCP	Doped TCP
Drop Volume	76 pL	76 pL
Saturation	110%	100%
Number of Print Head Passes	7	7
Print Head Speed	140 mm/s	140 mm/s
Layer Thickness	20 μm	30 μm
Feed Powder to Layer Thickness Ratio	3	3
Spread Speed	0.5 mm/s	0.5 mm/s

NIH-PA Author Manuscript

NIH-PA Author Manuscript

NIH-PA Author Manuscript

Table 2

Percent designed porosity and density of 3D printed scaffolds of pure and doped composition.

Interconnected Channel Size	Scaffold Type	Apparent Density of Struts	Total Open Pore Volume	Designed Pore Volume
1000um	Pure	89.9 (3.8)	51.14%	41.04%
	Doped	94.6 (3.8)	46.44%	
750um	Pure	91.2 (1.7)	44.31%	35.51%
	Doped	92.2 (4.1)	43.31%	
500um	Pure	91.4 (2.8)	35.86%	27.26%
	Doped	95.1 (4.72)	32.16%	

NIH-PA Author Manuscript

NIH-PA Author Manuscript

NIH-PA Author Manuscript

Table 3

Measurements of post sintered pore size in pure and SiO_2/ZnO doped TCP scaffolds.

	Pore Sizes After Sintering (μm)	
Pre Sintered Pore Size (μm)	**Pure**	**Doped**
1000	736.87 (2.99)	698.35 (3.48)
750	602.21 (4.14)	479.49 (2.71)
500	403.57 (6.55)	343.74 (8.26)